Stem Cell Reports
Report
ISSCR
OPEN ACCESS

Loss of MECP2 Leads to Activation of P53 and Neuronal Senescence

Minori Ohashi,[1,3,6] Elena Korsakova,[4,6] Denise Allen,[1] Peiyee Lee,[1] Kai Fu,[1] Benni S. Vargas,[1] Jessica Cinkornpumin,[1] Carlos Salas,[1] Jenny C. Park,[1] Igal Germanguz,[1] Justin Langerman,[2] Contantinos Chronis,[2] Edward Kuoy,[2] Stephen Tran,[5] Xinshu Xiao,[5] Matteo Pellegrini,[1] Kathrin Plath,[2,3,*] and William E. Lowry[1,3,4,*]

[1]Department of Molecular Cell and Developmental Biology, UCLA, Los Angeles, CA 90095, USA
[2]Department of Biological Chemistry, UCLA, Los Angeles, CA 90095, USA
[3]Eli and Edythe Broad Center for Regenerative Medicine, UCLA, Los Angeles, CA 90095, USA
[4]Molecular Biology Institute, UCLA, Los Angeles, CA 90095, USA
[5]Department of Integrative Biology and Physiology, UCLA, Los Angeles, CA 90095, USA
[6]Co-first author
*Correspondence: kplath@mednet.ucla.edu (K.P.), blowry@mcdb.ucla.edu (W.E.L.)
https://doi.org/10.1016/j.stemcr.2018.04.001

SUMMARY

To determine the role for mutations of *MECP2* in Rett syndrome, we generated isogenic lines of human induced pluripotent stem cells, neural progenitor cells, and neurons from patient fibroblasts with and without MECP2 expression in an attempt to recapitulate disease phenotypes *in vitro*. Molecular profiling uncovered neuronal-specific gene expression changes, including induction of a senescence-associated secretory phenotype (SASP) program. Patient-derived neurons made without MECP2 showed signs of stress, including induction of P53, and senescence. The induction of P53 appeared to affect dendritic branching in Rett neurons, as P53 inhibition restored dendritic complexity. The induction of P53 targets was also detectable in analyses of human Rett patient brain, suggesting that this disease-in-a-dish model can provide relevant insights into the human disorder.

INTRODUCTION

Rett syndrome is a disease associated with loss of function mutations in the gene MECP2, which was originally identified as encoding a methylated DNA binding protein (Chen et al., 2001; Meehan et al., 1992). Patient symptoms include microcephaly, intellectual disability, facial dysmorphia, and seizure activity (Bird, 2008). Studies in murine models recapitulate many of the patient phenotypes and have recently identified a role for Mecp2 particularly in inhibitory neurons (Tomassy et al., 2014). These studies demonstrated that loss of MECP2 can lead to defects in transcription (Chen et al., 2003; Lee et al., 2014), dendritic branching (Zhou et al., 2006), nuclear size (Chen et al., 2001), and AKT signaling (Li et al., 2013).

MECP2 has also been described as a transcription factor with specific targets (Chen et al., 2003; Zhou et al., 2006), and more broadly as either a transcriptional activator (Li et al., 2013) or repressor (Cross et al., 1997; Nan et al., 1997). However, despite decades of research on MECP2, it is still unclear how mutations in this protein lead to patient symptoms (Chen et al., 2001; Marchetto et al., 2010). To confirm findings made in other models and further study these in a human system, some have turned to modeling Rett syndrome *in vitro* by taking advantage of disease-in-a-dish approaches. This involves making human induced pluripotent stem cells (hiPSCs) from patient somatic cells, or using genome engineering to introduce mutations into wild-type (WT) human pluripotent stem cells. In the current study, we also sought to mitigate the effect of genetic background and variability of differentiation by taking advantage of several isogenic lines of hiPSCs that either express the WT allele or the mutant allele leading to cells that express or lack MECP2 (Tchieu et al., 2010). This allowed for detailed molecular analyses of hiPSCs, neural progenitor cells (NPCs), and neurons with and without MECP2 under the same genetic background. In comparing neurons from Rett patients as well as those with *MECP2* silenced by small interfering RNA (siRNA), it is clear that loss of MECP2 leads to induction of P53 and senescence, potentially opening an avenue of investigation for this intellectual disability syndrome.

RESULTS

A Human Model of Rett Syndrome *In Vitro*

Cognizant of the fact that differentiation from hPSCs is highly variable across individual lines, culture conditions, and time, we developed an isogenic model to study Rett syndrome *in vitro* to remove the confound of genetic background (Tchieu et al., 2010). Because female patients with Rett syndrome are usually heterozygous for mutant alleles of *MECP2*, fibroblasts isolated from these patients display a mosaic pattern where roughly half the cells express either the mutant or WT allele. This is shown in Figure 1A, where fibroblasts isolated from two patients with distinct mutant alleles of *MECP2* (R982 and R567) showed that roughly half

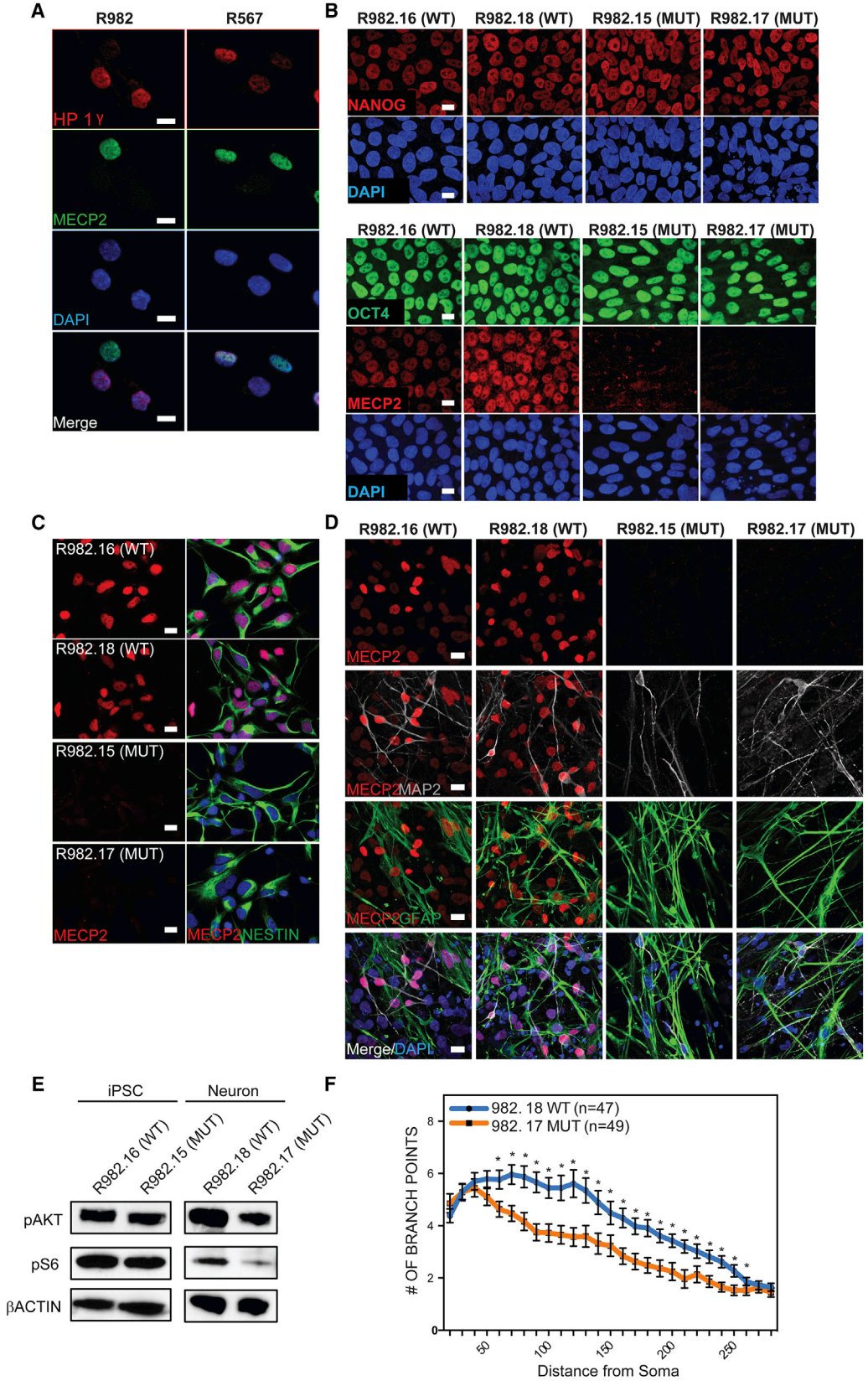

(legend on next page)

the cells expressed MECP2 while the other half lacked detectable amounts of this protein. Patient descriptions are provided in Figure S1. Reprogramming to iPSCs using a small set of transcription factors has been shown to happen at the clonal level, such that individual reprogramming events in single fibroblasts generate isolated hiPSC clones (Winkler et al., 2010). Therefore, reprogramming of mosaic fibroblast cultures from two different patients generated single hiPSC clones that either expressed MECP2 protein or lacked it (Figure 1B) (method described in a previous study; Sahakyan et al., 2016). In addition, our work and that of others has shown that under standard conditions, the inactive X chromosome in human fibroblasts does not reactivate upon reprogramming to the pluripotent state (Tchieu et al., 2010), which is distinct from murine reprogramming (Maherali et al., 2007).

Thus, we were able to create multiple lines of hiPSCs with and without MECP2 from individual patients and thereby control for differences in genetic background (shown in Figure 1B are clones made from patient 982; clones from 567 look similar). The hiPSCs generated from fibroblasts of both patients appeared to be unaffected by the lack of MECP2, expressed all appropriate markers, and successfully generated teratomas upon injection into the testes of immunocompromised mice, consistent with previous hiPSC models for loss of MECP2 (Figure S2A) (Cheung et al., 2011; Hotta et al., 2009). Lack of MECP2 in patient-derived cells and specificity of antibody was also confirmed by western blot (Figure S2B).

Importantly, we never observed reactivation of the silenced X chromosome that would have resulted in re-expression of the WT allele of *MECP2* in any cultures regardless of differentiation status or passage. This is consistent with previous data showing that, despite evidence for erosion of isolated portions of the silenced X chromosome (Mekhoubad et al., 2012), many portions of the inactivated X remain silenced even through reprogramming or differentiation (Patel et al., 2017; Tchieu et al., 2010). To measure the effect of any potential XCI erosion, we performed a DNA methylation analysis on the X chromosome on the lines from patient 982. This analysis showed that while some erosion of XCI was detectable across the X chromosome, there was not a significant difference between any of the lines (Figure S3A), and methylation at the *MECP2* locus specifically was unchanged between the lines (Figure S3B).

As Rett syndrome primarily afflicts the nervous system and MECP2 is most highly expressed in neurons, we first generated NPCs from all of the hiPSCs lines following standard protocols (Patterson et al., 2012). Across at least two lines per patient with and without MECP2, we measured the rate of neuralization, the morphology of NPCs, and expression of typical marker genes. We were unable to detect consistent differences in these properties between multiple clones of both WT and MECP2 null lines derived from both patients (Figures 1C and S2C). Furthermore, the growth rate of NPCs with and without MECP2 was not consistently different in NPCs made from either patient (Figure S2D). Next, the NPCs were further differentiated by a non-directed differentiation approach that yields both neurons and glia (growth factor withdrawal; Patterson et al., 2012) (Figure 1D). All NPCs from both patients produced neurons and glia at the same rate (Figures S2E and S2F).

Previous studies have also shown that loss of MECP2 in neurons can lead to a decrease in AKT signaling (Li et al., 2013). A similar pattern was observed here in mutant neurons generated from Rett patient hiPSCs as measured by phosphorylation of AKT and S6, while hiPSCs themselves did not seem to be affected by loss of MECP2 (Figure 1E). Dendritic complexity has been shown extensively to be reliant on MECP2 expression in various models of Rett syndrome, and we found a statistically significant decrease in complexity in neurons made in the absence of MECP2 by Sholl assay (Figure 1F). In addition, we observed qualitative differences in basic neuronal morphology between WT and mutant neurons, where the neurons lacking MECP2 had shorter, thicker processes, and their soma was not as well defined.

Figure 1. Generation of the Isogenic Model of Rett Syndrome *In Vitro*

(A) Fibroblasts isolated from Rett syndrome patients (R982 and R567) heterozygous for MECP2 mutations exhibit a mosaic pattern of MECP2 expression due to random XCI.

(B) Multiple isogenic hiPSC lines were produced from patient 982 with a typical Yamanaka protocol yielding individual isogenic clones with and without MECP2 expression from the same patient, as judged by NANOG and OCT4 staining.

(C) Specification of hiPSCs derived from patient 982 toward neural progenitor cells yielded homogeneous cultures of NPCs with and without MECP2.

(D) Terminal differentiation of NPCs derived from patient 982 toward neurons and glia by growth factor withdrawal as measured by immunostaining for MAP2 and GFAP.

(E) MECP2+ and MECP2− hiPSCs and neurons were assayed by western blot with antibodies that recognize the active forms of Akt and its downstream target S6.

(F) Sholl assay of dendritic complexity was performed on WT versus MUT neurons derived from patient 982.

*$p < 0.05$ according to Student's t test. Bar graphs represent means ± SEM. Scale bars on images indicate 10 μm.

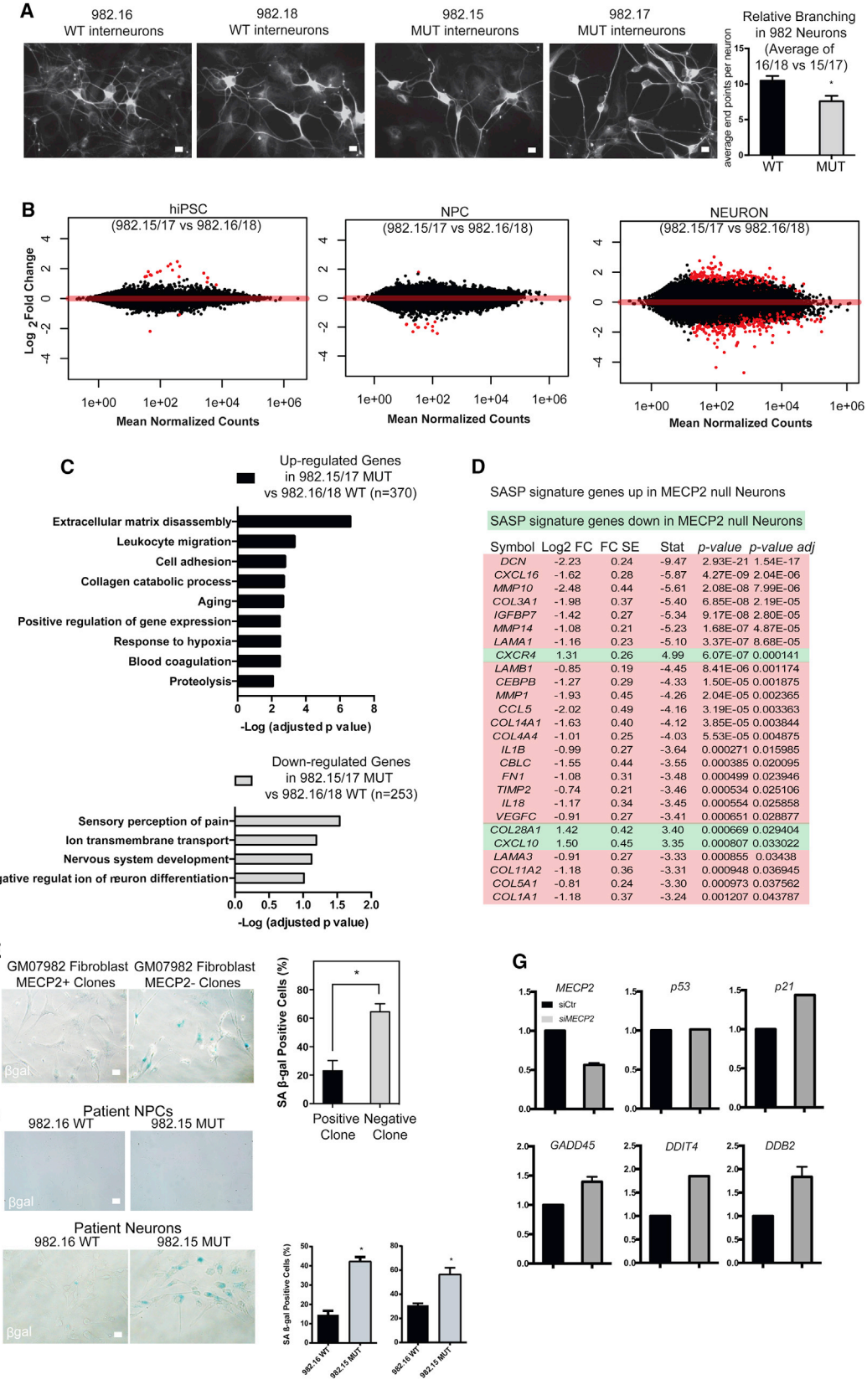

(legend on next page)

Loss of MECP2 Affects the Transcriptome of Neurons

It has been suggested that loss of MECP2 only affects gene expression in neurons as opposed to the hPSCs and NPCs from which they were derived (Li et al., 2013). We sought to determine whether gene expression was affected in hiPSCs, NPCs, or neurons in this patient-derived *in vitro* model. To optimize the search for molecular effects of loss of MECP2 in neurons, we generated defined neuronal cultures by following the newly established 3i (three inhibitor) method to create interneurons (Figure 2A) (Maroof et al., 2013). Interneurons are particularly relevant in the study of Rett syndrome as interneuron-specific deletion of *Mecp2* in mice recapitulates many of the disease symptoms (Ito-Ishida et al., 2015; Tomassy et al., 2014). We validated the quality of differentiation at each step by immunostaining for markers typical of particular cell types (SOX2, SOX1, and NESTIN as well as FOXG1 and NKX2.1 for NPCs; and Tuj1, MAP2, and GABA for interneurons) in both WT and MUT cultures followed by quantification (Figures S4A and S4B). While methods for derivation from pluripotent stem cells are effective at making interneurons, these cultures are not pure. As such, we first ensured that the proportion of neurons present in the cultures for comparison were not consistently different (Figure S4C). We then assessed whether interneurons lacking MECP2 also showed diminished dendritic branching. In fact, in patient-derived interneurons made by 3i, defects in dendritic branching as measured by the number of endpoints were clearly observed (Figure 2A).

We therefore proceeded with deep RNA sequencing (RNA-seq; >120 million reads per sample) of hiPSC, NPC, and interneuron cultures. With such sequencing depth, it was possible to analyze the RNA-seq reads for the known mutations present in the patients from which these lines were made (Figure S4D). This analysis demonstrated that each line studied expressed strictly either the WT or mutant allele of *MECP2*, and that XCI status was unchanged even after extensive differentiation to neurons. We quantified the expression level of *MECP2* in WT cells across these three stages of development and found that the average reads per kilobase of transcript per million mapped reads RPKM was 3.1 for hiPSCs, 4.3 for NPCs, and 7.75 for interneuron-enriched cultures. This is consistent with consensus that MECP2 is enriched in neuronal cells, but also demonstrates that it could potentially be relevant to hiPSC and NPC physiology as well. However, high stringency analyses (false discovery rate <0.05) of the RNA-seq data yielded very few gene expression changes due to loss of MECP2 in hiPSCs or NPCs derived from Rett patients (Figure 2B), consistent with Li et al. (2013). On the other hand, interneuron cultures made from patient 982 showed many gene expression changes when comparing two individual WT and MUT clones (Figure 2B). Gene ontology analysis uncovered many neuronal physiology-related pathways that were downregulated due to loss of MECP2 in neurons, while genes associated with extracellular remodeling and cell migration appeared to be induced (Figure 2C).

Probing the RNA-seq data, we also found that MECP2 null interneuron cultures showed a strong increase in a group of genes that are known to be induced by senescent cells, known as the senescence-associated secretory program (SASP). The vast majority of SASP genes that were changed in MECP2 null neurons were upregulated as opposed to downregulated, suggesting a robust pattern of SASP induction (Figure 2D). The only previous report linking MECP2 loss to senescence was performed by partial silencing of this protein in mesenchymal stem cells, but the results were consistent with those shown here for patient-derived MECP2 null fibroblasts (Squillaro et al., 2010). The induction of SASP was intriguing in light of the fact that, while attempting to make clones of fibroblasts from patients with Rett syndrome, we repeatedly found that clones lacking MECP2 did not expand well after passage (14 MECP2 null clones were created, none expanded), while clones expressing the WT allele expanded without a problem (42 MECP2+ clones were created, we attempted to expand four of them, and all four expanded).

To determine whether MECP2 null fibroblasts encounter senescence, we performed an assay to detect endogenous

Figure 2. Loss of MECP2 Is Associated with Differential Gene Expression in Neurons

(A) Immunostaining neurons generated from patient 982 for TuJ1, a neuronal-specific marker. Right: quantification of dendritic complexity by counting endpoints.

(B) Volcano plots of differentially expressed genes (DEGs) in hiPSCs, NPCs, and neurons.

(C) Gene ontological analysis of DEGs increased versus decreased in MECP2 null neurons.

(D) An examination of SASP genes in neurons.

(E) Patient skin-derived clones of fibroblasts lacking MECP2 showed strong β-gal activity, while those of WT fibroblasts did not.

(F) Top: the senescence assay applied to neural progenitors derived from Rett patients did not show significant senescence activity. Bottom: patient-derived neuronal cultures showed a strong increase in the absence of MECP2 (quantification across independent lines shown on the right).

(G) RT-PCR for P53 targets after siRNA treatment of WT neurons.

Bar graphs represent means ± SEM. *p < 0.05. Scale bars on images indicate 10 μm.

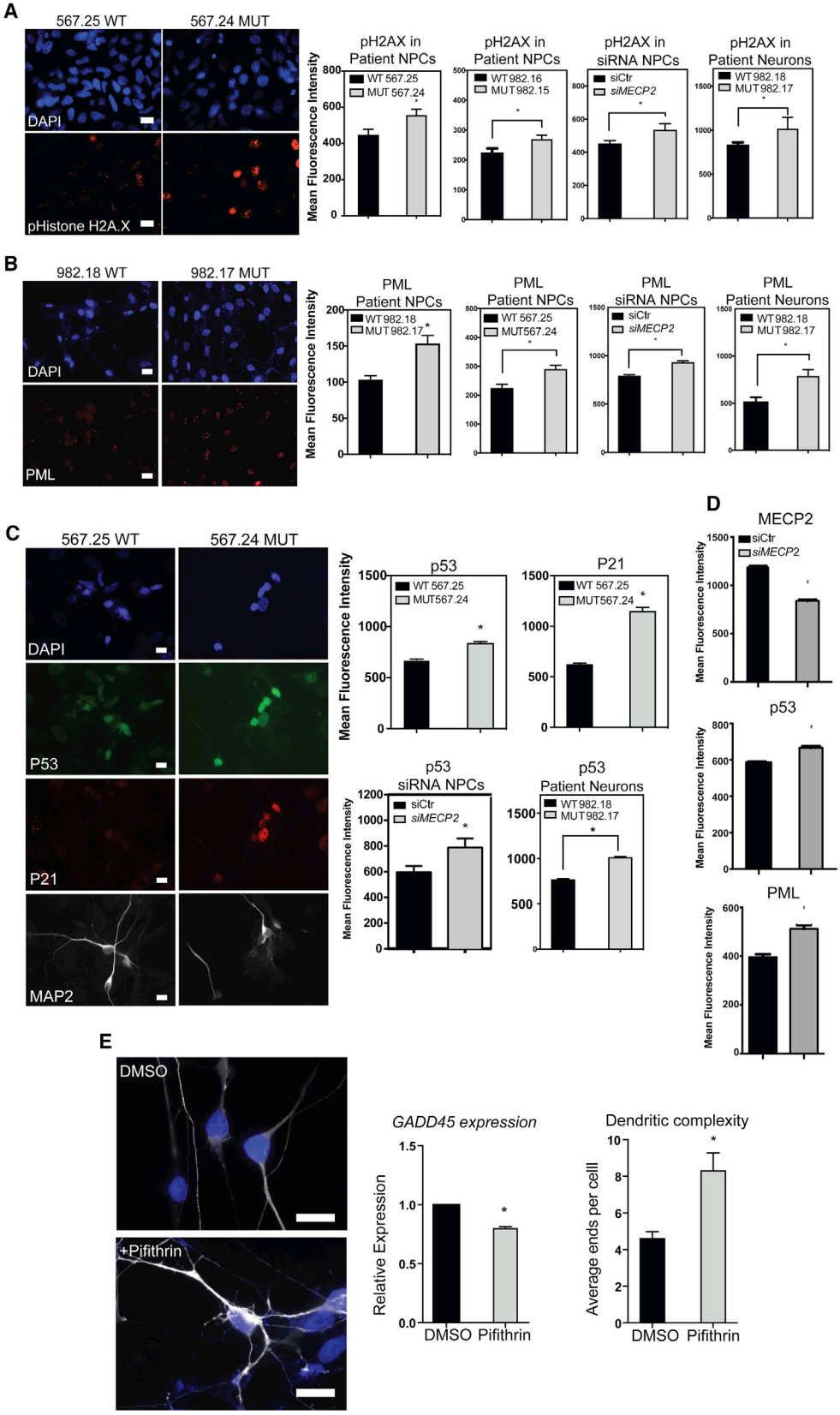

(legend on next page)

beta-galactosidase activity, which is known to be a hallmark of this process (Wang et al., 2013). Indeed, MECP2 null fibroblasts showed strong activity in this senescence assay (Figure 2E). We did not encounter such difficulties with clonal expansion once hiPSCs or hiPSC-derived NPCs were made from patients, presumably because during reprogramming, telomerase is strongly induced to restore telomere length at least beyond the critical threshold (Marion et al., 2009; Suhr et al., 2009). In fact, our RNA-seq data showed that hiPSCs made from patients had very high expression of *TERT*, and NPCs still expressed moderate levels, while neurons did not express appreciable levels (average RPKM for *TERT*: hiPSC, 8.8; NPC, 1.6; neuron, 0.006). Importantly, the same endogenous galactosidase activity assay on interneurons showed a dramatic increase in senescence activity in neurons lacking MECP2 (Figure 2F). These data indicate that loss of MECP2 leads to not only induction of SASP but also a *bona fide* senescence program in neurons.

Induction of P53 in the Absence of MECP2

Cellular senescence programs are known to be regulated by P53, which can then activate various response pathways downstream, such as DNA repair and apoptosis (Vaziri and Benchimol, 1996). Interestingly, P53 induction due to telomere shortening was previously shown to cause defects in dendritic branching (Ferron et al., 2009), which is also the dominant phenotype in Rett syndrome. To begin to look for hallmarks of P53 induction in the absence of MECP2, we performed RT-PCR for P53-related targets in cells with silencing of *MECP2* by siRNA (Figure S4E). This assay suggested that decreased MECP2 levels led to induction of P53-related target genes such as *P21*, *GADD45*, *DDIT4*, and *DDB2* (Figure 2G).

To determine the effect of loss of MECP2 in relation to cell-stress pathways at the protein level, we performed immunostaining for H2AX, PML, P53, and P21 in neurons with and without MECP2. Staining for each of these markers showed strong increases in expression/levels of these markers of cell stress in patient-derived NPCs, neurons, and also after silencing of *MECP2* in both NPCs and neurons (Figures 3A–3D). WT NPCs with silencing of *MECP2* by siRNA and neurons lacking MECP2 also showed clear induction of these marks.

Blocking Induction of P53 Can Rescue Dendritic Branching Defects Due to Loss of MECP2

Previous evidence from a murine model of telomere shortening as a result of loss of telomerase complex (TERT) led to defects in dendritic branching, and this effect was strictly dependent on induction of P53 (Ferron et al., 2009). A more recent study also showed that experimentally aging the neural lineage with telomerase inhibition led to neurons with signs of aging, including reduced dendritic branching (Vera et al., 2016). Therefore, we posited that inhibition of P53 in MECP2 null neurons could potentially restore appropriate dendritic branching. To determine whether blocking the action of P53 could improve dendritic branching in MECP2 null interneurons, we took advantage of Pifithrin-α, a potent inhibitor of P53 target gene activation (Bassi et al., 2002). Treatment of MECP2 null interneurons with Pifithrin-α showed evidence of P53 inhibition as measured by RT-PCR for *GADD45* (Vaziri and Benchimol, 1996), a target gene important for DNA repair (Figure 3E). After 24–48 hr of P53 inhibition by Pifithrin-α, MECP2 null interneurons appeared to adopt an improved neuronal morphology typified by increased physical distinction between the soma and neurites, longer, thinner neurites, as well as increased dendritic branching as shown and quantified in Figure 3E. These data provide evidence that neurons without MECP2 induce P53 activity, which then inhibits the formation of complex neuronal processes.

To determine whether any of the phenotypes discovered in this *in vitro* model of Rett syndrome have relevance to patients afflicted with the disease, we acquired tissue specimens from Rett patients and age-matched controls. We first quantified the degree of chimerism of female Rett patient neurons due to skewing of X chromosome inactivation to determine the relative ratio of neurons that express MECP2 versus those that did not. Some of the Rett patient brains showed roughly 75% of neurons lacked MECP2, while others appeared to have less than 25% MECP2 null neurons (Figure 4A).

Figure 3. Loss of MECP2 Leads to Induction of DNA Damage and P53

(A) Immunostaining of patient NPCs, NPCs with siRNA against MECP2, and patient neurons showed a strong increase in H2aX in the absence of MECP2.

(B) Immunostaining of patient NPCs, NPCs with siRNA against MECP2, and patient neurons.

(C) Immunostaining for P53 and p21, a target of P53.

(D) Immunostaining after siRNA silencing of MECP2 in WT neuronal cultures.

(E) Treatment of MECP2 null neurons with DMSO or Pifithrin, followed by immunostaining with antibody for TuJ1 shows a change in dendritic branching. Bottom left: RT-PCR for *GADD45*, a P53 target gene, showed that Pifithrin reduced P53 activity. Bottom right: quantification of branching phenotype across three independent experiments.

*$p < 0.05$ according to Student's t test. Bar graphs represent means ± SEM. Scale bars on images indicate 10 μm.

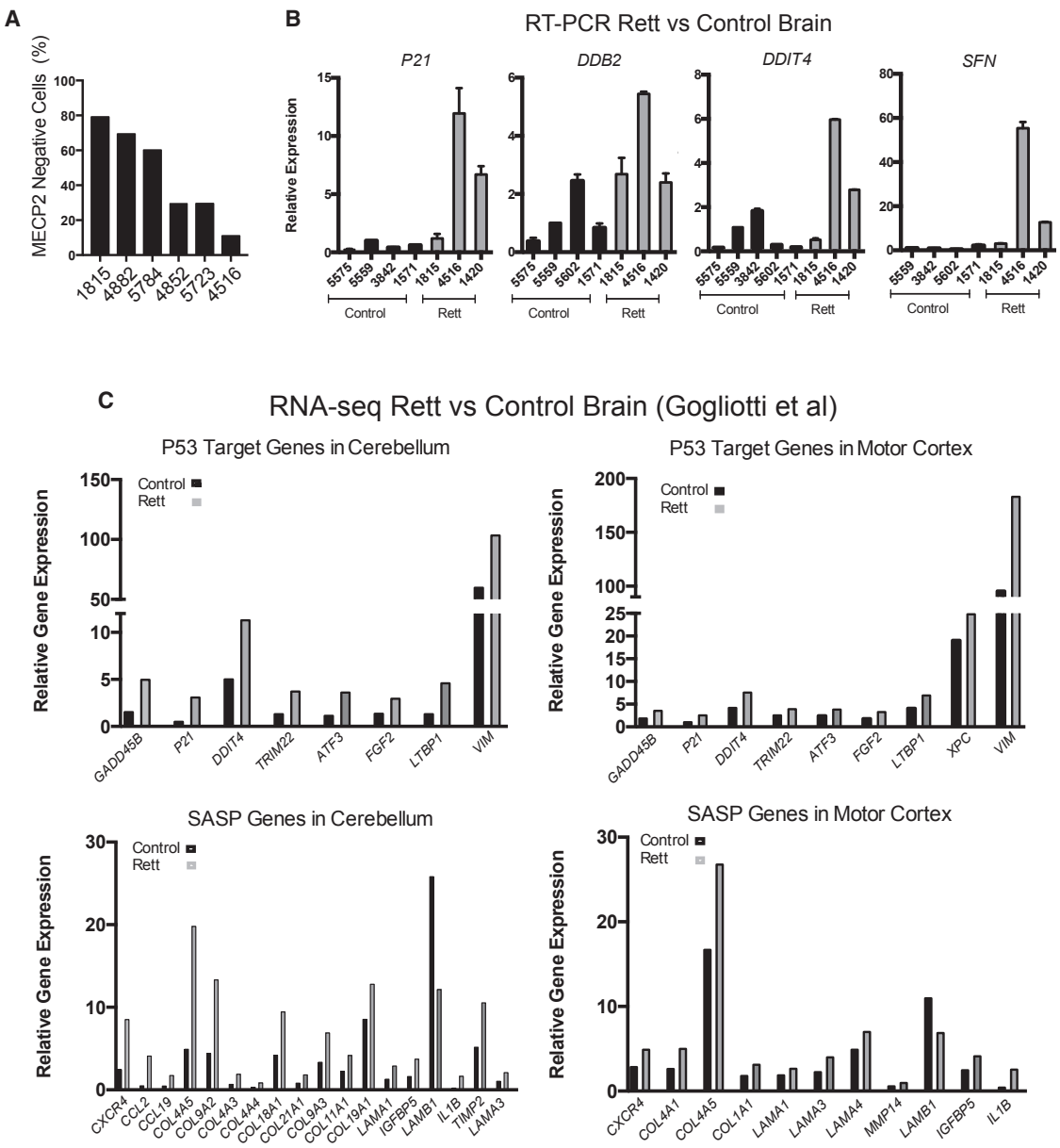

Figure 4. Evidence for P53 Induction in Rett Patient Neurons in Human Brain

(A) Each Rett brain sample was assessed for the percentage of neurons with and without expression of MECP2 by immunostaining.

(B) RT-PCR on RNA isolated from Rett brain versus age-matched control brains for P53 targets.

(C) A re-analysis of data published by Gogliotti et al. (2018). Shown are a sample of P53 targets and SASP genes found on lists of genes upregulated in Rett brain. All of these differentially expressed genes were derived using a corrected p value (false discovery rate) <0.05 from at least n = 5 samples from control and Rett brains.

Bar graphs represent means ± SEM.

We performed RT-PCR on samples from some of these brains to determine whether they showed signs of increased P53 activity. To ensure accurate RNA representation, we first assessed the quality of the RNA from these frozen tissues, and only proceeded with RT-PCR in samples that showed an RIN (RNA integrity number) value above 5. All the Rett patient brains we processed for RT-PCR showed induction of canonical P53 target genes (identified in Wei et al., 2006), consistent with what was observed in the patient-derived neurons *in vitro* (Figure 4B). Recently, a new study was published that isolated brain tissue from Rett patients and control subjects to

perform an RNA-seq profile to characterize changes specific to Rett motor cortex or cerebellum. Using data provided in that study, we found that many direct P53 targets (as defined in Wei et al., 2006) and SASP signature genes were upregulated in the Rett brains in both the motor cortex and the cerebellum (Figure 4C).

DISCUSSION

Taken together, these data demonstrate that loss of MECP2 leads to clear signs of stress such as H2AX deposition, P53/P21 induction, and initiation of a senescence program, all of which suggest that neurons in Rett syndrome could be in suboptimal health, leading to neurophysiological defects such as dendritic arborization (Zhou et al., 2006). While one paper suggested that RNAi-mediated silencing of *MECP2* could promote senescence in mesenchymal cells (Squillaro et al., 2010), decades of work on Rett syndrome have not uncovered a role for MECP2 in relation to senescence in a wide variety of models such as various transgenic mouse lines, human patient postmortem analyses, and *in vitro* human models.

These results also raise the question of whether senescence could be common to the etiologies of other intellectual disability syndromes. The phenotypes described here show a striking similarity to those observed in hiPSCs and neural derivatives made from patients with immunodeficiency, centromeric region instability, and facial anomalies syndrome (ICF) syndrome (Yehezkel et al., 2013). Two independent studies showed that ICF patient-derived hiPSCs displayed telomere shortening that was coupled to senescence of somatic derivatives such as fibroblasts. ICF syndrome only partially overlaps with Rett syndrome in terms of patient phenotypes, but is caused by mutations in DNMT3B, a *de novo* DNA methyltransferase (Linhart et al., 2007). These findings together are highly relevant as DNMT3B is a key *de novo* methyl transferase to create methylated DNA (5mC), which is the substrate for Tet oxygenase's to create 5-hydroxmethylated DNA (5hmC), which is known to be strongly bound by MECP2 (Mellen et al., 2012). Recently, another study showed that deletion of Tet enzymes, which are critical to generate the 5hmC mark, led to shortened telomeres (Yang et al., 2016), which is known to lead to P53 activation.

Another possible interpretation of these data is that instead of a failure to mature, Rett syndrome neurons instead show aspects of premature aging. The fact that MECP2 null neurons show induction of aging-related genes, including P53 targets, and induce senescence pathways are consistent with this idea (Tan et al., 2014). On the other hand, while Rett patients suffer from a post-natal cognitive decline, and long-term survivors show phenotypes associated with Parkinson disease (Zoghbi, 2016), the typical phenotypes presented in young female patients are not consistent with premature aging. Whether the physiological response to loss of MECP2 is truly akin to premature aging or whether patients suffer from effects that are unrelated to aging is worthy of continued investigation.

EXPERIMENTAL PROCEDURES

Generation of Isogenic Rett Syndrome iPSCs

Reprogramming was performed as described (Lowry et al., 2008).

Generation of Teratomas

Generation of teratomas was previously described (Lindgren et al., 2011).

Differentiation *In Vitro* and Analysis

Neural specification with neural rosette derivation, neuroprogenitor (NPC) purification, and further differentiation to neurons and glia were performed as described previously (Patterson et al., 2012, 2014).

Immunofluorescence and Image Quantification

Immunofluorescence was performed as described previously (Patterson et al., 2014) and is described in detail in the Supplemental Information.

RT-qPCR

RT-PCR with real-time PCR measurement was carried out on a Roche 480 as described (Patterson et al., 2012, 2014). The primer sequences are available in the Supplemental Information.

siRNA Gene Silencing

All knockdown experiments were performed as described previously (Patterson et al., 2014).

β-Galactosidase Senescence Assay

β-Galactosidase senescence assay was performed using the Senescence β-Galactosidase Staining Kit from Cell Signaling. The number of blue cells and number of total cells were quantified using the Cell Counter plugin in ImageJ.

Quantification of Dendritic Arborization

The stained cells were then imaged at 20×, and dendritic arbors of individual cells were traced using the Simple Neurite Tracer plugin for ImageJ. The number of process ends per cell were counted using the Cell Counter plugin for ImageJ. The number of process ends per cell are presented as mean ends per cell ± SEM.

RNA Expression Profiling

RNA-seq was performed as described previously (Gu et al., 2016). These data are available from NIH dataset GEO: GSE107399.

SUPPLEMENTAL INFORMATION

Supplemental Information includes Supplemental Experimental Procedures and four figures and can be found with this article online at https://doi.org/10.1016/j.stemcr.2018.04.001.

AUTHOR CONTRIBUTIONS

M.O., E.K., D.A., P.L., K.F., B.S.V., J.C., C.S., J.C.P., I.G., J.L., C.C., E.K., and S.T. provided data through experimentation. M.O., E.K., and W.E.L. contributed to writing the manuscript. X.X., M.P., K.P., and W.E.L. provided financial support for this work.

ACKNOWLEDGMENTS

We would like to acknowledge the helpful discussions and insight on this manuscript with Gail Mandel (OHSU). This work was funded by training grants to M.O. (NIH-Virology and Gene Therapy, UCLA), P.L. (CIRM, UCLA), C.S. (CIRM-Bridges, Cal-State-Northridge), and D.A. (HHURP, UCLA). W.E.L. was supported by a Rose Hills Scholar award through the Eli and Edythe Broad Center for Regenerative Medicine. W.E.L. and K.P. were supported by NIH (P015P01GM099134). This research was also supported by the Allen Distinguished Investigator Program and the Paul G. Allen Frontiers Group, and a March of Dimes Scholar Award (6-FY17-406).

Received: September 15, 2017
Revised: March 30, 2018
Accepted: April 3, 2018
Published: May 8, 2018

REFERENCES

Bassi, L., Carloni, M., Fonti, E., Palma de la Pena, N., Meschini, R., and Palitti, F. (2002). Pifithrin-alpha, an inhibitor of p53, enhances the genetic instability induced by etoposide (VP16) in human lymphoblastoid cells treated in vitro. Mutat. Res. *499*, 163–176.

Bird, A. (2008). The methyl-CpG-binding protein MeCP2 and neurological disease. Biochem. Soc. Trans. *36*, 575–583.

Chen, R.Z., Akbarian, S., Tudor, M., and Jaenisch, R. (2001). Deficiency of methyl-CpG binding protein-2 in CNS neurons results in a Rett-like phenotype in mice. Nat. Genet. *27*, 327–331.

Chen, W.G., Chang, Q., Lin, Y., Meissner, A., West, A.E., Griffith, E.C., Jaenisch, R., and Greenberg, M.E. (2003). Derepression of BDNF transcription involves calcium-dependent phosphorylation of MeCP2. Science *302*, 885–889.

Cheung, A.Y., Horvath, L.M., Grafodatskaya, D., Pasceri, P., Weksberg, R., Hotta, A., Carrel, L., and Ellis, J. (2011). Isolation of MECP2-null Rett syndrome patient hiPS cells and isogenic controls through X-chromosome inactivation. Hum. Mol. Genet. *20*, 2103–2115.

Cross, S.H., Meehan, R.R., Nan, X., and Bird, A. (1997). A component of the transcriptional repressor MeCP1 shares a motif with DNA methyltransferase and HRX proteins. Nat. Genet. *16*, 256–259.

Ferron, S.R., Marques-Torrejon, M.A., Mira, H., Flores, I., Taylor, K., Blasco, M.A., and Farinas, I. (2009). Telomere shortening in neural stem cells disrupts neuronal differentiation and neuritogenesis. J. Neurosci. *29*, 14394–14407.

Gogliotti, R., Fisher, N., Stansley, B., Jones, C., Lindsley, C., Conn, J., and Niswender, C. (2018). Total RNA-sequencing of Rett syndrome autopsy samples identifies the M4 muscarinic receptor as a novel therapeutic target. J. Pharmacol. Exp. Ther. *365*, 291–300.

Gu, W., Gaeta, X., Sahakyan, A., Chan, A.B., Hong, C.S., Kim, R., Braas, D., Plath, K., Lowry, W.E., and Christofk, H.R. (2016). Glycolytic metabolism plays a functional role in regulating human pluripotent stem cell state. Cell Stem Cell *19*, 476–490.

Hotta, A., Cheung, A.Y., Farra, N., Vijayaragavan, K., Seguin, C.A., Draper, J.S., Pasceri, P., Maksakova, I.A., Mager, D.L., Rossant, J., et al. (2009). Isolation of human iPS cells using EOS lentiviral vectors to select for pluripotency. Nat. Methods *6*, 370–376.

Ito-Ishida, A., Ure, K., Chen, H., Swann, J.W., and Zoghbi, H.Y. (2015). Loss of MeCP2 in parvalbumin-and somatostatin-expressing neurons in mice leads to distinct Rett syndrome-like phenotypes. Neuron *88*, 651–658.

Lee, W., Yun, J.M., Woods, R., Dunaway, K., Yasui, D.H., Lasalle, J.M., and Gong, Q. (2014). MeCP2 regulates activity-dependent transcriptional responses in olfactory sensory neurons. Hum. Mol. Genet. *23*, 6366–6374.

Li, Y., Wang, H., Muffat, J., Cheng, A.W., Orlando, D.A., Loven, J., Kwok, S.M., Feldman, D.A., Bateup, H.S., Gao, Q., et al. (2013). Global transcriptional and translational repression in human-embryonic-stem-cell-derived Rett syndrome neurons. Cell Stem Cell *13*, 446–458.

Lindgren, A.G., Natsuhara, K., Tian, E., Vincent, J.J., Li, X., Jiao, J., Wu, H., Banerjee, U., and Clark, A.T. (2011). Loss of Pten causes tumor initiation following differentiation of murine pluripotent stem cells due to failed repression of Nanog. PLoS One *6*, e16478.

Linhart, H.G., Lin, H., Yamada, Y., Moran, E., Steine, E.J., Gokhale, S., Lo, G., Cantu, E., Ehrich, M., He, T., et al. (2007). Dnmt3b promotes tumorigenesis in vivo by gene-specific de novo methylation and transcriptional silencing. Genes Dev. *21*, 3110–3122.

Lowry, W.E., Richter, L., Yachechko, R., Pyle, A.D., Tchieu, J., Sridharan, R., Clark, A.T., and Plath, K. (2008). Generation of human induced pluripotent stem cells from dermal fibroblasts. Proc. Natl. Acad. Sci. USA *105*, 2883–2888.

Maherali, N., Sridharan, R., Xie, W., Utikal, J., Eminli, S., Arnold, K., Stadtfeld, M., Yachechko, R., Tchieu, J., Jaenisch, R., et al. (2007). Directly reprogrammed fibroblasts show global epigenetic remodeling and widespread tissue contribution. Cell Stem Cell *1*, 55–70.

Marchetto, M.C., Carromeu, C., Acab, A., Yu, D., Yeo, G.W., Mu, Y., Chen, G., Gage, F.H., and Muotri, A.R. (2010). A model for neural development and treatment of Rett syndrome using human induced pluripotent stem cells. Cell *143*, 527–539.

Marion, R.M., Strati, K., Li, H., Tejera, A., Schoeftner, S., Ortega, S., Serrano, M., and Blasco, M.A. (2009). Telomeres acquire embryonic stem cell characteristics in induced pluripotent stem cells. Cell Stem Cell *4*, 141–154.

Maroof, A.M., Keros, S., Tyson, J.A., Ying, S.W., Ganat, Y.M., Merkle, F.T., Liu, B., Goulburn, A., Stanley, E.G., Elefanty, A.G., et al. (2013). Directed differentiation and functional maturation

of cortical interneurons from human embryonic stem cells. Cell Stem Cell *12*, 559–572.

Meehan, R.R., Lewis, J.D., and Bird, A.P. (1992). Characterization of MeCP2, a vertebrate DNA binding protein with affinity for methylated DNA. Nucleic Acids Res. *20*, 5085–5092.

Mekhoubad, S., Bock, C., de Boer, A.S., Kiskinis, E., Meissner, A., and Eggan, K. (2012). Erosion of dosage compensation impacts human iPSC disease modeling. Cell Stem Cell *10*, 595–609.

Mellen, M., Ayata, P., Dewell, S., Kriaucionis, S., and Heintz, N. (2012). MeCP2 binds to 5hmC enriched within active genes and accessible chromatin in the nervous system. Cell *151*, 1417–1430.

Nan, X., Campoy, F.J., and Bird, A. (1997). MeCP2 is a transcriptional repressor with abundant binding sites in genomic chromatin. Cell *88*, 471–481.

Patel, S., Bonora, G., Sahakyan, A., Kim, R., Chronis, C., Langerman, J., Fitz-Gibbon, S., Rubbi, L., Skelton, R.J.P., Ardehali, R., et al. (2017). Human embryonic stem cells do not change their X inactivation status during differentiation. Cell Rep. *18*, 54–67.

Patterson, M., Chan, D.N., Ha, I., Case, D., Cui, Y., Handel, B.V., Mikkola, H.K., and Lowry, W.E. (2012). Defining the nature of human pluripotent stem cell progeny. Cell Res. *22*, 178–193.

Patterson, M., Gaeta, X., Loo, K., Edwards, M., Smale, S., Cinkornpumin, J., Xie, Y., Listgarten, J., Azghadi, S., Douglass, S.M., et al. (2014). let-7 miRNAs can act through notch to regulate human gliogenesis. Stem Cell Reports *3*, 758–773.

Sahakyan, A., Kim, R., Chronis, C., Sabri, S., Bonora, G., Theunissen, T.W., Kuoy, E., Langerman, J., Clark, A.T., Jaenisch, R., et al. (2016). Human naive pluripotent stem cells model X chromosome dampening and X inactivation. Cell Stem Cell *20*, 87–101.

Squillaro, T., Alessio, N., Cipollaro, M., Renieri, A., Giordano, A., and Galderisi, U. (2010). Partial silencing of methyl cytosine protein binding 2 (MECP2) in mesenchymal stem cells induces senescence with an increase in damaged DNA. FASEB J. *24*, 1593–1603.

Suhr, S.T., Chang, E.A., Rodriguez, R.M., Wang, K., Ross, P.J., Beyhan, Z., Murthy, S., and Cibelli, J.B. (2009). Telomere dynamics in human cells reprogrammed to pluripotency. PLoS One *4*, e8124.

Tan, F.C., Hutchison, E.R., Eitan, E., and Mattson, M.P. (2014). Are there roles for brain cell senescence in aging and neurodegenerative disorders? Biogerontology *15*, 643–660.

Tchieu, J., Kuoy, E., Chin, M.H., Trinh, H., Patterson, M., Sherman, S., Aimiuwu, O., Lingren, A., Zack, J.A., Clark, A., et al. (2010). Female human iPS cells retain an inactive X-chromosome. Cell Stem Cell *7*, 329–342.

Tomassy, G.S., Morello, N., Calcagno, E., and Giustetto, M. (2014). Developmental abnormalities of cortical interneurons precede symptoms onset in a mouse model of Rett syndrome. J. Neurochem. *131*, 115–127.

Vaziri, H., and Benchimol, S. (1996). From telomere loss to p53 induction and activation of a DNA-damage pathway at senescence: the telomere loss/DNA damage model of cell aging. Exp. Gerontol. *31*, 295–301.

Vera, E., Bosco, N., and Studer, L. (2016). Generating late-onset human iPSC-based disease models by inducing neuronal age-related phenotypes through telomerase manipulation. Cell Rep. *17*, 1184–1192.

Wang, Z., Wei, D., and Xiao, H. (2013). Methods of cellular senescence induction using oxidative stress. Methods Mol. Biol. *1048*, 135–144.

Wei, C.L., Wu, Q., Vega, V.B., Chiu, K.P., Ng, P., Zhang, T., Shahab, A., Yong, H.C., Fu, Y., Weng, Z., et al. (2006). A global map of p53 transcription-factor binding sites in the human genome. Cell *124*, 207–219.

Winkler, T., Cantilena, A., Metais, J.Y., Xu, X., Nguyen, A.D., Borate, B., Antosiewicz-Bourget, J.E., Wolfsberg, T.G., Thomson, J.A., and Dunbar, C.E. (2010). No evidence for clonal selection due to lentiviral integration sites in human induced pluripotent stem cells. Stem Cells *28*, 687–694.

Yang, J., Guo, R., Wang, H., Ye, X., Zhou, Z., Dan, J., Wang, H., Gong, P., Deng, W., Yin, Y., et al. (2016). Tet enzymes regulate telomere maintenance and chromosomal stability of mouse ESCs. Cell Rep. *15*, 1809–1821.

Yehezkel, S., Shaked, R., Sagie, S., Berkovitz, R., Shachar-Bener, H., Segev, Y., and Selig, S. (2013). Characterization and rescue of telomeric abnormalities in ICF syndrome type I fibroblasts. Front. Oncol. *3*, 35.

Zhou, Z., Hong, E.J., Cohen, S., Zhao, W.N., Ho, H.Y., Schmidt, L., Chen, W.G., Lin, Y., Savner, E., Griffith, E.C., et al. (2006). Brain-specific phosphorylation of MeCP2 regulates activity-dependent Bdnf transcription, dendritic growth, and spine maturation. Neuron *52*, 255–269.

Zoghbi, H.Y. (2016). Rett syndrome and the ongoing legacy of close clinical observation. Cell *167*, 293–297.

Stem Cell Reports, Volume *10*

Supplemental Information

Loss of MECP2 Leads to Activation of P53 and Neuronal Senescence

Minori Ohashi, Elena Korsakova, Denise Allen, Peiyee Lee, Kai Fu, Benni S. Vargas, Jessica Cinkornpumin, Carlos Salas, Jenny C. Park, Igal Germanguz, Justin Langerman, Contantinos Chronis, Edward Kuoy, Stephen Tran, Xinshu Xiao, Matteo Pellegrini, Kathrin Plath, and William E. Lowry

Supplemental information

Extended Materials and Methods

Generation of isogenic Rett Syndrome iPSCs

Two primary fibroblast lines GM17567 (1461A>G in the gene encoding methyl-CpG binding protein 2 (MECP2)), and GM07982 (frameshift mutation, 705delG, in the gene encoding methyl-CpG binding protein 2 (MECP2)), from patients with Rett Syndrome were obtained from Coriell Cell Repositories (Described in Fig S1). After 8-12 hours, the cells were infected with reprogramming lentivirus that harbors polycystronic human Yamanaka factors (Oct4, Klf4, Sox2, cMyc) in DMEM medium containing 10ug/ml of polybrene and incubated overnight at 37^{o}C in 5% CO2 incubator. On day 6, the culturing media was changed to human ES media containing DMEM/F12 supplemented with L-glutamine, nonessential amino acids (NEAA), penicillin-streptomycin, knockout serum replacement (Invitrogen), and 10 ng/ml basic FGF. Cells were cultured in hiPSC media until iPSC-like colonies were formed.

Generation of teratomas

Generation of teratoma was previously described(Lindgren et al., 2011). Briefly, a single incision was made in the peritoneal cavity of adult SCID mice and the testis was explanted through the incision site. Approximately 60,000 iPSC in a volume of 50 ml 0.5X Matrigel (BD) were transplanted into the testis using a 27-gauge needle. Four to six weeks after surgery, mice were euthanized and the tumors removed for histology.

Differentiation in vitro and analysis

Neural specification with neural rosette derivation, neuroprogenitor (NPC) purification, and further differentiation to neurons and glia were performed as described previously (Karumbayaram et al., 2009; Patterson et al., 2011; Patterson et al., 2014). For spontaneous terminal neuronal differentiation by growth factor withdrawal, NPC cultures were subjected to growth factor withdrawal (removal of EGF and FGF) and cultured in basic medium (DMEMF12 + N2 + B27) with three quarter exchange of media every three days. Neural differentiation efficiency was analyzed four weeks after growth factor withdrawal by counting the number of cells positive for neuronal markers (MAP2 and Tuj1) over the total number of cells visualized by DAPI. NPCs were transfected with *DCX-GFP* reporter one day prior to differentiation using Lipofectamine 2000 (Invitrogen). Sholl analysis of DCX-GFP positive neurites were also measured using ImageJ. All data values were presented as mean +/- SEM. For directed differentiation of interneurons, iPSCs were grown on plates coated with matrigel (Corning) until 80% confluency with mTeSR (Stem Cell Technologies). Cells were then treated with DMEM/F12 (GIBCO) containing NEAA (GIBCO), GlutaMAX (GIBCO), bovine serum albumin (Sigma-Aldrich), ß-mercaptoethanol (Sigma-Aldrich), N2 (GIBCO), B27 (GIBCO), SB431542 (10uM; Cayman Chemical), LDN-193189 (100nM; Cayman Chemical) and XAV939 (2uM; Cayman Chemical) later transitioning to the media containing sonic hedgehog (20ng/mL; R&D) and purmorphamine (1uM; Cayman Chemical) as previously described (Maroof et al., 2013). Cells were further differentiated into interneurons with neurobasal medium (GIBCO) containing N2 (GIBCO), B27 (GIBCO), ascorbic acid (Sigma-Aldrich), GlutaMAX (GIBCO), bovine serum albumin (Sigma-Aldrich), ß-mercaptoethanol (Sigma-Aldrich),

neurotrophin-3 (10ng/mL; R&D), brain-derived neurotrophic factor (10ng/mL; R&D), and glial cell-derived neurotrophic factor (10ng/mL; R&D).

Western blot

Cells were lysed on ice with RIPA buffer (Pierce) that contains Halt Protease Inhibitor Cocktail (Thermo Fisher Scientific) and Halt Phosphatase Inhibitor Cocktail (Thermo Fisher Scientific). The total protein concentration was measured using BCA Protein Assay Kit (Thermo Fisher Scientific) following the manufacturer's protocol. Supernatant was electrophoresed onto NuPAGE 4-12% Bis-Tris Protein Gels (Invitrogen) using MOPS running buffer (Invitrogen). The membrane was blocked with 5% non-fat milk for 1 hr and incubated overnight with primary antibodies at 4°C.

Immunofluorescence and image quantification

Cells on coverslips were washed with PBS, fixed in 4% paraformaldehyde for 15 min at room temperature, blocked for 1 hr at room temperature with 10% serum and 0.1% Triton-X-100, then incubated overnight at 4 °C with primary antibodies. Following primary antibody incubation, the coverslips were incubated with Alexa Fluor (Invitrogen) or Jackson Immunoresearch secondary antibodies at room temperature for 1 hr. Cells were counterstained with DAPI and mounted in Prolong Gold (ThermoFisher). Antibodies used include the following: mouse anti-OCT3/4 (1:100, Santa Cruz Biotechnology Inc., sc-5279), rabbit anti-SOX2 (1:300, Cell Signaling Technology, 3579), rabbit anti-Nanog (1:100, Cell Signaling Technology, 4903), mouse anti-Tra-1-81 (1:250, Chemicon, MAB4381), mouse anti-NESTIN (1:1000, Neuromics, MO15012), chicken anti-MAP2 (1:2000, Biolegend, PCK-554P), chicken anti-GFAP (1:2000, Abcam, ab4647), rabbit

anti-Tubulin β3 (1:500, Covance, MMS-435P), mouse anti-P53 (1:500, Cell Signaling, 2524), rabbit anti-p21 (1:250, Santa Cruz, sc-397), mouse anti-PML (1:100, Santa Cruz, sc-9862), mouse anti-phospho-Histone H2A.X (1:2000, EMD Millipore, 05-636), rabbit anti-5hmc (1:100, Active Motif, 39791), rabbit anti MECP2 (1:1000, Diagenode, pAb-052-050), rabbit anti Foxg1 (1:1000, Abcam, ab18259), and mouse anti NKX2.1 (1:300, Novocastra, NCL-L-TTF-1). Secondary antibodies conjugated with Alexa 488, 568, 594, 647 (1:500, Life Technologies, A-21203, A21202, A31571, A-21207) were used. Mean intensity or a number of foci were quantified using ImageJ (http://rsb.info.nih.gov/ij/). At least 100 cells per condition were used for each independent experiment.

RT-qPCR

RNA from cultured cells was collected using the RNeasy Mini Kit from Qiagen according to the manufacturer's instructions. RNA with an A260/A280 ratio in between 1.8 and 2.0 as well as an A260/A230 ratio in between 2.0 and 2.2 was used. RNA was then reverse transcribed using the Super Script III First-Strand cDNA Synthesis kit with Random Hexamers (Invitrogen) according to the manufacturer's instructions. Quantitative PCR was performed using SYBR Green master mix (Roche). Reactions were performed in duplicate and duplicate CT values were averaged and then used for standard ΔΔCT analysis. Expression levels were normalized to beta actin.

Primer Sequences

MECP2	*GCTCTGCTGGGAAGTATGATG*
MECP2	*ATGTGTCGCCTACCTTTTCG*
P53_F	*GCCCAACAACACCAGCTCCT*
P53_R	*CCTGGGCATCCTTGAGTTCC*

P21-F	*AAAGAAGAACGGAGCGAACA*
P21-R	*CTCCGCTCAATTTCCAAGAG*
GADD45G-F	*TACGCTGATCCAGGCTTTCT*
GADD45G-R	*AACAGGCTGAGCTTCTCCAA*
DDIT4_F	*GTTTGACCTCTCCACCAGCCT*
DDIT4_R	*GCACACAAGTGTTCATCCTCAGG*
DDB2_F	*TCACTTCCAGCACCTCACAC*
DDB2_R	*ACGTCGATCGTCCTCAATTC*
SFN_F	*GTGTGTCCCCAGAGCCATGG*
SFN_R	*ACCTTCTCCCGGTACTCACG*

Data collection and statistical analysis

All the experimental data (RT-qPCR, immunostaining, ß-Galactosidase Senescence Assay) were presented as mean +/- SEM based on at least three biological replicates from independent experiments. Student's t-tests were applied to data with two groups. ANOVA analyses were used for comparisons of data with greater than two groups. A *p-value* < 0.05 was considered as statistically significant.

siRNA gene silencing

All knockdown experiments were performed using trilencer siRNAs (from OriGene Technologies) and RNAimax (ThermoFisher) in Opti-MEM media (ThermoFisher). Trilencers were used at a concentration of 20 nM. Transfection media was prepared and then 500,000 cells were plated on top of the transfection media in 6-well plates. The medium was changed to normal NPC media the next day and cells were collected for analysis at the time points indicated.

ß-Galactosidase Senescence Assay

ß-Galactosidase Senescence Assay was performed using the Senescence β-Galactosidase Staining Kit from Cell Signaling according to manufacturer's instructions. Briefly, the cells were fixed on coverslips, incubated with X-gal overnight at 37°C, then mounted on glass slides and imaged using a brightfield microscope. The number of blue cells and number of total cells were quantified using the Cell Counter plugin in ImageJ.

Quantification of Dendritic Arborization

Neuronal cultures were immunostained for Tuj1 in order to identify mature neurons and visualize entire cells. The stained cells were then imaged at 20x and dendritic arbors of individual cells were traced using the Simple Neurite Tracer plugin for ImageJ. The number of process ends per cell were counted using the Cell Counter plugin for ImageJ. The number of process ends per cell are presented as mean ends per cell +/- SEM. Means were compared using the Student's t-Test for data with two groups.

RNA expression profiling

Libraries were prepared according to the manufacturers guidelines using The TruSeq V2 kit (Illumina). For RNA sequencing, the datasets were mapped with RASER and HISAT2. Genes were defined by the exon union from the hg19 ensembl annotations. The function of DESeq in DESeq2 package was used to first normalize the gene read counts data and then identified the differentially expressed genes. The MA plot was generated with the function of plotMA in DESeq2 package. Q-value of 0.05 is regarded as the stringent cutoff of calling DEGs while p-value less than 0.05 is regarded as the low stringency cutoff. For the meta-chromosome plot of DEGs, all the chromosomes (except chromosome Y) were first divided equally into 20bins with different length, and then the number of DEGs in

each bin was counted. GO analysis was performed using DAVID. These data are available from NIH GEO Dataset GSE107399.

Figure S1. Description of patient source for fibroblasts for reprogramming. Supplementary to Figure 1.

Patient data, taken from NIH BioBrainBank repository

Patient 982

Description:
RETT SYNDROME; RTT
METHYL-CPG-BINDING PROTEIN 2; MECP2
Affected: Yes
Gender: Female
Age: 25 YR (At Sampling)

Remarks: Clinically affected; microcephaly; scoliosis diagnosed at age 12; severe kyphoscoliosis at age 25; early milestones were slow; started losing skills at age 2; currently severely retarded; behavioral phenotype includes hand wringing that began at age 2 and became more intense; no sleep problems; no self-injurious behavior; abnormal EEG; CT scan at age 25 showed evidence of atrophy; donor subject carries a frameshift mutation, 705delG, in the gene encoding methyl-CpG binding protein 2 (MECP2); see GM07983 lymphoblast.

Patient data 567

Description:
RETT SYNDROME; RTT
METHYL-CPG-BINDING PROTEIN 2; MECP2
Affected:Yes
Gender:Female
Age:5 YR (At Sampling)

Clinically affected; onset between 15-20 months of age; seizures began at age 3; never walked independently; began to develop repetitive hand movements at 28 months; no hand use; small feet; language regression at 18 months; some sleep problems; nonverbal; significantly abnormal EEG; swallowing difficulties, reflux, and breathing problems; teeth grinding; decelerating head circumference; growth retardation; seizures; donor subject has a missense mutation (A>G) at nucleotide 1461 (1461A>G) in the gene encoding methyl-CpG binding protein 2 (MECP2), resulting in a substitution of a tryptophan for a stop codon at codon 487 [TER487TRP (X487W)].

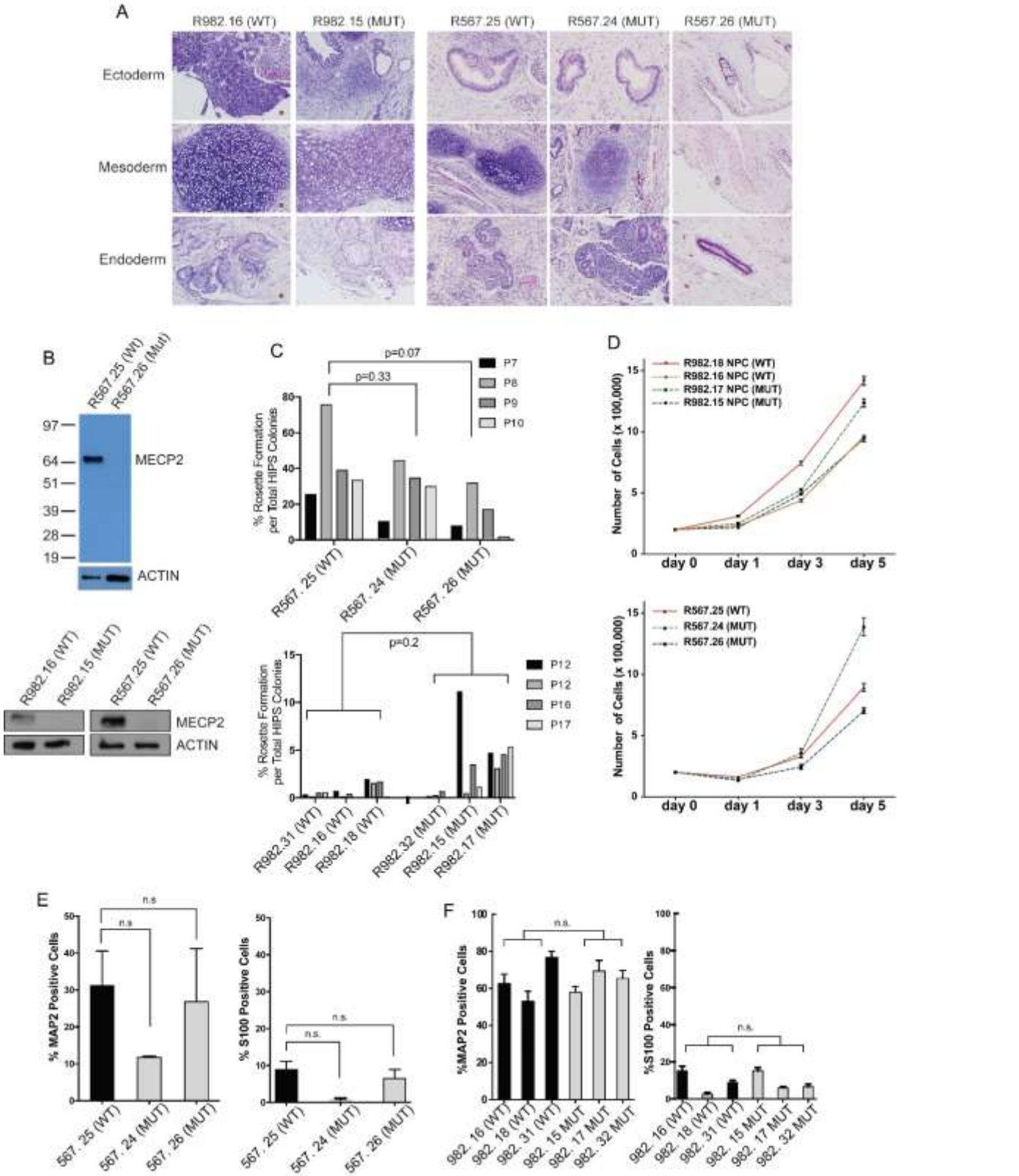
A
R982.16 (WT)
R982.15 (MUT)
R567.25 (WT)
R567.24 (MUT)
R567.26 (MUT)
Ectoderm
Mesoderm
Endoderm
B
R567.25 (Wt)
R567.26 (Mut)
97
64
51
39
28
19
MECP2
ACTIN
R982.16 (WT)
R982.15 (MUT)
R567.25 (WT)
R567.26 (MUT)
MECP2
ACTIN
C
p=0.07
p=0.33
P7
P8
P9
P10
% Rosette Formation per Total HIPS Colonies
R567. 25 (WT)
R567. 24 (MUT)
R567. 26 (MUT)
p=0.2
P12
P12
P16
P17
% Rosette Formation per Total HIPS Colonies
R982.31 (WT)
R982.16 (WT)
R982.18 (WT)
R982.32 (MUT)
R982.15 (MUT)
R982.17 (MUT)
D
R982.18 NPC (WT)
R982.16 NPC (WT)
R982.17 NPC (MUT)
R982.15 NPC (MUT)
Number of Cells (x 100,000)
day 0
day 1
day 3
day 5
R567.25 (WT)
R567.24 (MUT)
R567.26 (MUT)
Number of Cells (x 100,000)
day 0
day 1
day 3
day 5
E
n.s
n.s
% MAP2 Positive Cells
567. 25 (WT)
567. 24 (MUT)
567. 26 (MUT)
n.s.
n.s.
% S100 Positive Cells
567. 25 (WT)
567. 24 (MUT)
567. 26 (MUT)
F
n.s.
%MAP2 Positive Cells
982. 16 (WT)
982. 18 (WT)
982. 31 (WT)
982. 15 MUT
982. 17 MUT
982. 32 MUT
n.s.
%S100 Positive Cells
982. 16 (WT)
982. 18 (WT)
982. 31 (WT)
982. 15 MUT
982. 17 MUT
982. 32 MUT

Figure S2. Validation of disease in a dish model for Rett Syndrome. Supplementary to Figure 1.

A, Teratoma assay was performed to establish pluripotency of hiPSCs made from Rett patient fibroblasts. The resulting tumors each showed evidence of differentiation towards all three embryonic germ layers. **B,** NPCs were produced from isogenic hiPSCs of Rett patient, and assessed by western blot to validate loss of MECP2 and specificity of antibody. Top panel shows that the antibody only recognizes MECP2. Bottom panel shows that in NPCs from both patients, individual clones either express or lack MECP2. **C**, The ability of hiPSCs to generate NPCs was assayed in Rosette formation assay. Lack of MECP2 did not affect rosette formation across multiple lines from both patients. N=4 independent experiments. *p value < 0.05 according to student's t test (for patient R567) or ANOVA (for patient R982). Bar graphs represent mean +/- SEM. **D**, Growth curves show that loss of MECP2 does not affect proliferation of NPCs made from either patient. **E**, 3 weeks of growth factor withdrawal drives NPCs to differentiate into neurons and glia as measured here by immunostaining for MAP2/Tuj1 or S100/GFAP in patient 567 derived cultures. There was no consistent difference in differentiation potential across lines from either patient. N=2 independent experiments. Bar graphs represent mean +/- SEM. **F**, Patient 982 derived cultures also do not show dramatic differences in the presence of neurons or astrocytes as measured by MAP2 and S100. N=3 independent experiments. Bar graphs represent mean +/- SEM. Scale Bars represent 20 microns.

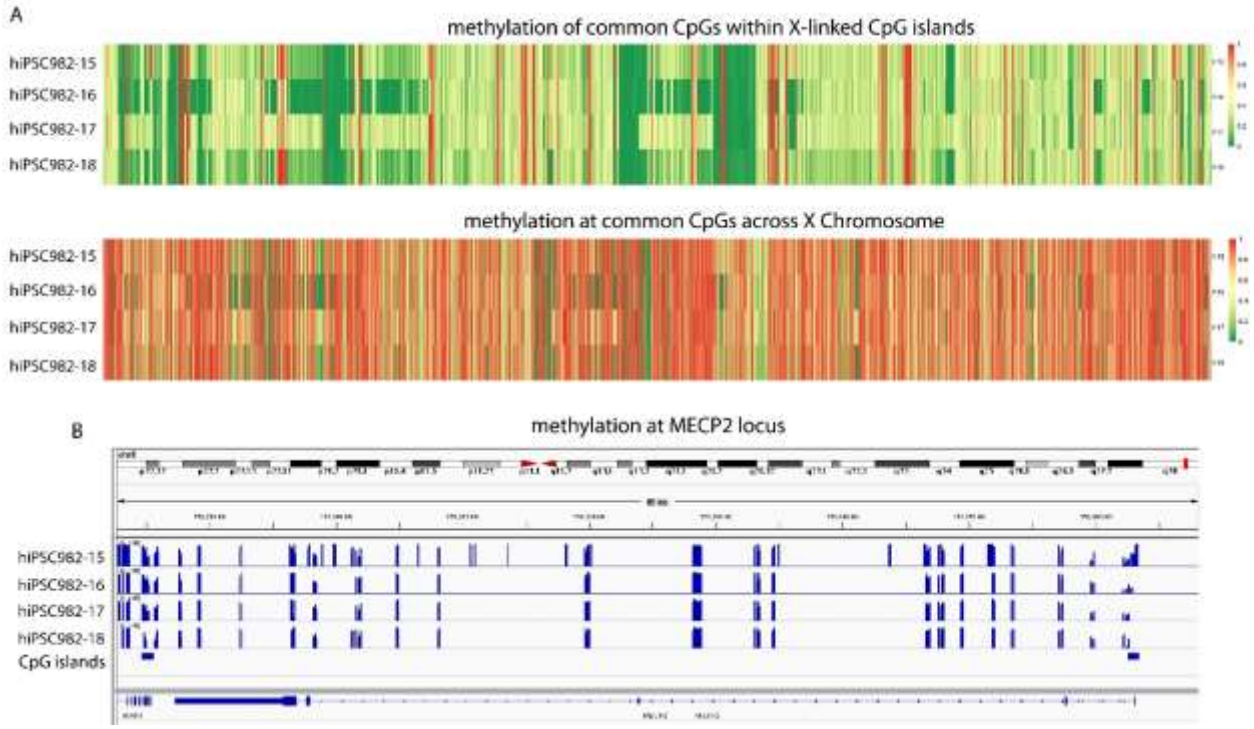

Figure S3. Methylation analysis to measure XCI erosion in hiPSC lines made from Rett Patients. Supplementary to figure 1.

A, The silencing of the X chromosome is accompanied by the gain of DNA methylation at CpG islands (CGIs). We utilized reduced representation bisulfite sequencing (RRBS) to examine methylation levels across the X chromosome in indicated hiPSC lines. Methylation level of 1 indicates 100% methylation and 0 absence of methylation. Top: Heatmap of RRBS-based methylation levels for CpGs within X-linked CGIs showing that most CGIs are hemi-methylated (intermediate methylation level) indicative of XCI on one X chromosome and no methylation on the other (which results in hemi-methylation when measured across both X chromosomes). Erosion (no methylation) is only seen for a small subset of CGIs (compare to data in (Patel et al., 2017)). Only CpGs with coverage across all samples are shown (including across Patel et al samples). Bottom: As above, except for all CpGs on the X chromosome with coverage in all samples, demonstrating the globally high methylation level in all hiPSCs. **B,** IgV view of the

methylation data within the MECP2 locus. The CGI of MECP2 is indicated and hemi-methylated in all hiPSC lines, indicative of XCI at this locus. RRBS and data analysis was performed as described in(Patel et al., 2017).

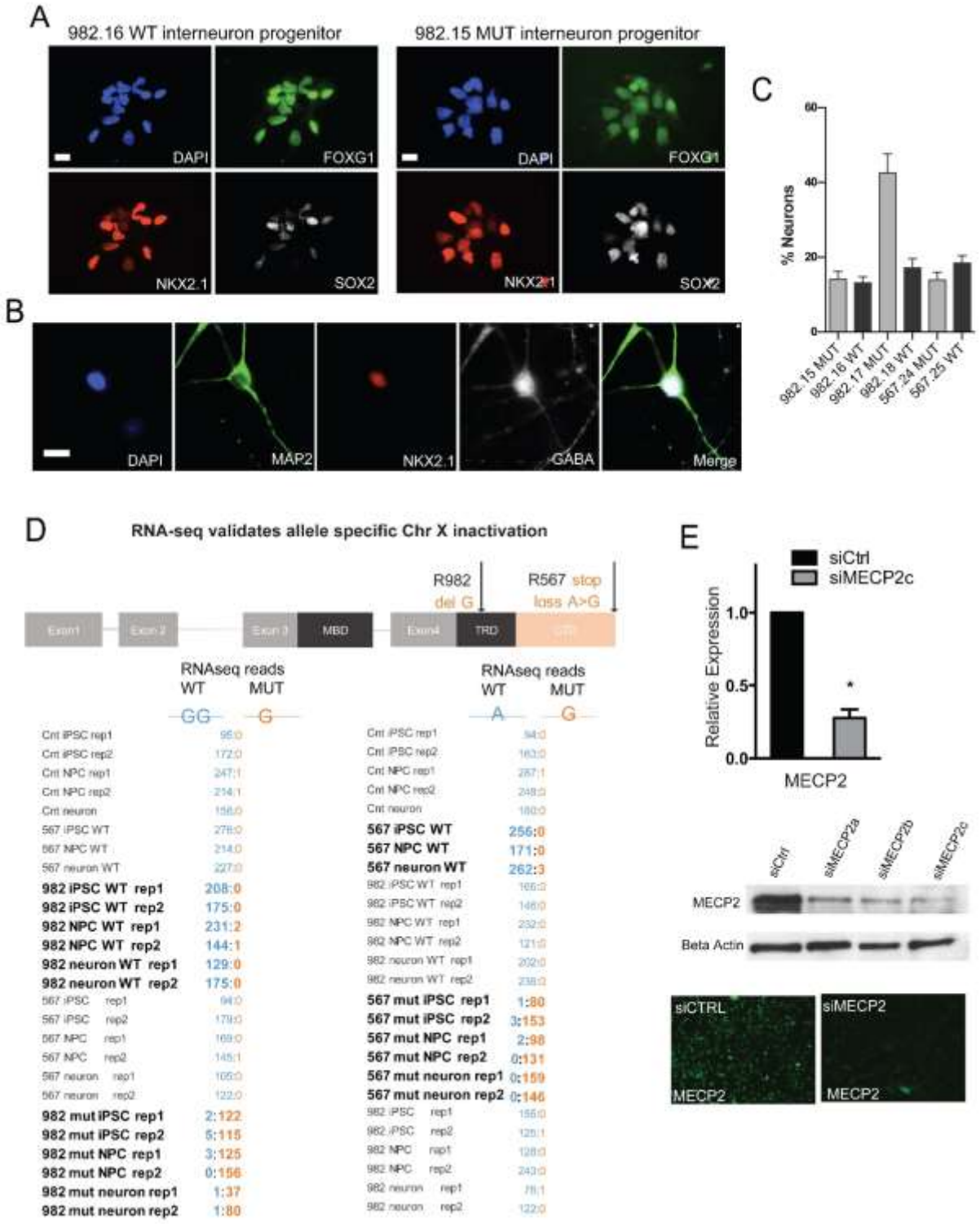

Figure S4. RNA-seq analysis to determine the relative ration of WT versus MUT transcripts of MECP2 in Rett patient derived lines. Supplementary to figure 2.

A and B, immunostaining to demonstrate the efficiency of directed differentiation towards neural progenitors (A) and then onto interneurons (B) with markers typical of each stage. **C,** Quantification of the percentage of interneurons in the cultures used to perform the RNA-seq, as measured by immunostaining. **D,** Detection of WT and MUT transcripts from each of the lines indicated demonstrated a clear bias towards individual alleles in each patient derived line. This analysis indicates XCI status for each allele, and demonstrates that XCI status is unchanged, even after differentiation to neurons. **E**, MECP2 was downregulated by RNA interference, quantified by RT-PCR (left), for protein by western blot (middle), and as demonstrated by immunostaining for MECP2 (right). N=3 independent experiments. *p value < 0.05 according to student's t test. Bar graphs represent mean +/- SEM. Scale bars represent 10 microns.

Patel, S., Bonora, G., Sahakyan, A., Kim, R., Chronis, C., Langerman, J., Fitz-Gibbon, S., Rubbi, L., Skelton, R.J.P., Ardehali, R.*, et al.* (2017). Human Embryonic Stem Cells Do Not Change Their X Inactivation Status during Differentiation. Cell Rep *18*, 54-67.